

Research Paper

Spatial Variations in the Characteristics of Oscillated and Non-Oscillated Solar Bright Points in Active Regions and Coronal Holes

Rayhaneh Sadeghi¹ · Ehsan Tavabi^{*2}

¹ Physics Department, Payame Noor University, Tehran, Iran;
email: rayhane.sadeghi@gmail.com

² Physics Department, Payame Noor University, Tehran, Iran;
*email: e_tavabi@pnu.ac.ir

Received: 27 January 2024; **Accepted:** 15 June 2024; **Published:** 18 June 2024

Abstract. In this study, researchers investigated the properties of oscillated and non-oscillated bright points (BPs) in different regions of the Sun, including active regions (ARs) and coronal holes (CHs). The findings revealed both differences and similarities among these BPs across the various regions. Firstly, the study observed that internetwork BPs in ARs exhibited higher damping times compared to network BPs. Additionally, internetwork BPs in ARs displayed wider ranges of maximum Doppler velocities in comparison to network BPs. Although both forms of BPs had comparable damping times, internetwork BPs demonstrated greater maximum Doppler velocities than network BPs. Moreover, the study provided insights into the damping behavior of BPs in different regions. Specifically, it was noted that the majority of network BPs in ARs exhibited overdamping, indicating that the damping effects were dominant. On the other hand, in CHs, internetwork BPs displayed overdamping behavior, suggesting a similar dominance of damping effects. In contrast, oscillated network BPs in CHs exhibited critical damping behavior, implying a balance between damping and driving forces. It is important to emphasize that the physical principles underlying BP damping may vary depending on the local plasma conditions and magnetic surroundings. Overall, this study highlights the diverse characteristics of BPs in different solar regions, shedding light on their damping times, maximum Doppler velocities, and damping behaviors. These findings contribute to our understanding of the intricate dynamics and plasma conditions occurring in different areas of the Sun, providing valuable insights into the complex nature of solar phenomena.

Keywords: Sun, Bright points, Oscillations

1 Introduction

Solar bright points (BPs) are small-scale magnetic structures in the solar photosphere and chromosphere that play a crucial role in energy transmission and solar atmospheric heating. Their oscillatory behavior has been a topic of interest for several decades, with the first observations of oscillations reported by [1]. These oscillations are often associated with

* Corresponding author

This is an open access article under the **CC BY** license.



the emergence of new magnetic flux and the cancellation of existing flux and can be observed in different period ranges. The oscillations are thought to be caused by propagating magneto-acoustic waves in loop systems associated with the BPs, or by recurrent magnetic reconnection. Coronal BPs exhibit quasi-periodic oscillations, which are linked to magnetic flux changes. They are caused by propagating slow magneto-acoustic waves and standing slow waves in the solar transition region. The oscillatory behavior is particularly prominent above BP-like structures in the quiet Sun. Interface Region Imaging Spectrograph (IRIS) BPs are tiny bright features detected at the interface region between the Sun's photosphere and the corona. These BPs are assumed to be the result of an interaction between the magnetic field and the plasma in the area, leading to plasma heating through various mechanisms. The interaction between the magnetic field and plasma can lead to plasma heating through various mechanisms, including the rapid redistribution of energy in magnetically confined equilibrium plasma, the generation of magnetic fields in warm plasma by the non-stationary ponderomotive force of an electromagnetic wave, and the simulation of plasma flow interaction with arched magnetic fields [1–21].

Scientists expect to obtain a better knowledge of how the Sun's magnetic field and plasma interact, as well as how energy is distributed throughout the Sun's atmosphere, by examining IRIS BPs. The data has already yielded fresh insights into the dynamics of the Sun's interface region and the function of the magnetic field in creating the observed features. Solar BPs are crucial for both practical and scientific purposes, as their energy can impact Earth's atmosphere and damage communication and navigation systems. Understanding these features can help predict space weather and mitigate its impacts on our technologies. Oscillations, or periodic fluctuations in brightness over time, can provide valuable insights into how magnetic fields and plasma behave in the Sun's atmosphere [7,13,22–30].

Research on solar BPs has revealed a significant percentage of oscillations, with 16 out of 23 coronal BPs exhibiting decayless kink oscillations, with periods ranging from 1 to 8 minutes. These oscillations are subject to various damping mechanisms, including thermal effects, mass flows, resonant damping in non-uniform media, and partial ionization effects. In the case of solar-type stars, acoustic mode damping and excitation are influenced by stochastic processes. The presence of oscillations in coronal BPs has been observed, with some displaying a damped oscillatory behavior. By evaluating the structure of magnetic fields and the presence of these oscillations at solar BPs, scientists can gain important insights into the mechanisms that regulate the Sun's activity and use the observations' data to validate and refine models of the Sun's magnetic field and plasma. Network BPs, located mostly in the sun's network regions, have high magnetic fields, while inter-network BPs arise in zones of the sun with lower magnetic fields. While solar BPs are known to oscillate, this is not true for all BPs. Different types of solar BPs have diverse features, and while some oscillate, others do not. This paper presents a statistical study of oscillated and non-oscillated BPs based on high-resolution observations obtained from the *IRIS*, offering a comprehensive and quantitative comparison between these two categories of BPs, considering their spatial, temporal, and spectral properties [5,13,17,28,30–41].

2 Observation

NASA's *IRIS* mission aims to capture high-resolution images and spectra at specific wavelengths of light to explore the interface region between the sun's chromosphere and corona. The data provides insights into energy and matter movement through the sun's atmosphere, particularly at the chromosphere-corona boundary. The *IRIS* has a primary mirror with a focal length of 3320 mm and a slit-jaw imaging technology that captures images at four

UV light wavelengths. Its spectrograph uses a novel architecture to capture spectral lines in a restricted wavelength range with high spatial and temporal precision. The spectrograph provides a range of spatial resolution between 0.33 to 0.4 arcseconds, corresponding to approximately 240 kilometers on the Sun's surface. It can accurately detect plasma velocity with a precision of 1 to more than 5 km/s, depending on the temporal resolution of the data series [18,42,42,43].

3 Method

The identification algorithm employed in this study aimed to accurately detect and classify Bright Points (BPs) in solar images. The algorithm utilized a combination of image processing techniques and machine learning approaches to achieve its objective. Firstly, a series of pre-processing steps were applied to enhance the quality of the solar images and facilitate subsequent analysis. These steps included noise reduction, contrast enhancement, and normalization.

Next, the algorithm employed a segmentation technique to isolate potential BPs from the rest of the image. Various segmentation methods could be used, such as thresholding, region growing, or edge detection, depending on the characteristics of the BPs and the images under consideration. Once the initial segmentation was performed, the algorithm proceeded to extract relevant features from the segmented regions. These features could include intensity-based measures, texture descriptors, shape properties, or spatial information. The selection of appropriate features was crucial for distinguishing BPs from the surrounding background and other solar features. After feature extraction, a machine learning model was trained using a labeled dataset. The dataset consisted of solar images with annotated BPs, where each BP was associated with its corresponding class label. The model could be trained using various machine learning algorithms, such as support vector machines (SVM), random forests, or convolutional neural networks (CNN). In this case, a Convolutional Neural Network (CNN) was used.

During the training phase, the algorithm learned to recognize patterns in the extracted features and associate them with the appropriate class labels (i.e., whether that was a BP or not). The model's parameters were adjusted iteratively to optimize its performance and increase its ability to accurately classify BPs. Once the model was trained, it could be applied to solar images for BP identification. The algorithm processed each image, performed the pre-processing steps, segmented the regions of interest, extracted features, and passed them through the trained model for classification. The output provided information about the presence or absence of BPs in the analyzed regions of the solar images. The performance of the identification algorithm was evaluated using appropriate metrics. These metrics provided insights into the algorithm's ability to correctly identify BPs and distinguish them from other solar features or artifacts. The identification algorithm utilized a combination of image processing techniques and machine learning approaches. It involved pre-processing, segmentation, feature extraction, and machine learning model training to accurately detect and classify BPs in solar images. The algorithm's performance was evaluated using various metrics, ensuring its effectiveness in identifying BPs and contributing to our understanding of solar phenomena.

This study employed a supervised machine learning approach to segregate BPs from the solar disk's center. A training set was formed using SJIs obtained from the solar disk's center, including over 1,000 SJIs associated with quiet, active, and coronal hole regions. The selection of these images aimed to be representative of various observing conditions and modes, including different heliocentric angles. The model was trained using the annotated

training set, which included information about the brightness and coordinates of the bright features in the images. The model's performance was evaluated using an additional 100 SJIs, and the evaluation showed that the trained model achieved an accuracy of approximately 70% in identifying BPs. To measure accuracy, the number of correct predictions (true positives and true negatives) was compared to the total number of predictions made by the model. The data was divided into training, accuracy test, and test sets.

The identified BPs along the slit were selected for subsequent oscillation studies, allowing the focus on the regions of interest identified by the machine learning model. The CNN model was designed and trained on the annotated images, consisting of several layers, including convolutional, pooling, and fully connected layers. The CNN learned to identify patterns and features in the images, while the pooling layers reduced the spatial dimensions of the representation. The fully connected layers map the learned representation to the final output, which is the predicted brightness and coordinates of the bright features. The CNN model consists of an encoding path and a decoding path, connected by a bottleneck layer. The encoding path consists of three stages of convolutional layers with max pooling, the bottleneck layer consists of two convolutional layers with filters, and the decoding path consists of three stages of upsampling layers with convolutional layers. The output layer is a convolutional layer with a sigmoid activation function, producing a binary image of the predicted BPs. The total number of trainable parameters in the CNN model is approximately 1 million, and the input images are randomly augmented by flipping and rotating during training to increase diversity and reduce over-fitting [44–46].

The method developed for identifying and tracking Bright Points (BPs) in solar images has achieved high accuracy. The Mg II spectrum was used to identify BPs networks and inter-networks, using the Sadeghi and Tavabi (2022) technique (Figure 1). The image processing pipeline was developed to identify and track BPs in the *IRIS* observations, involving image enhancement, segmentation, feature extraction, and tracking. Advanced techniques, including machine learning algorithms, were employed to ensure precise identification and characterization of BPs. Wavelet analysis and Fourier analysis were employed to investigate the oscillatory behavior of BPs, classifying them into oscillated and non-oscillated groups based on significant oscillatory power in their intensity time series.

The proposed pipeline offers a flexible framework for the analysis of solar images, including image enhancement and segmentation steps. Techniques like contrast enhancement, noise reduction, and sharpening can be employed to enhance image quality, while segmentation techniques like threshold, region growing, edge detection, and morphological operations can be used. This flexibility allows researchers to customize and optimize the pipeline according to the dataset's characteristics and analysis objectives.

4 Results

The study investigates the properties of BPs in various regions of the Sun, including the AR, and CH areas. It focuses on the relationship between the maximum Doppler velocity and the damping per period of oscillated and non-oscillated BPs in the solar network and internetwork. The research reveals a clear distinction between oscillated and non-oscillated BPs, with the former exhibiting significantly higher oscillatory power in the 3-5 minute period range. Oscillated BPs also showed a higher degree of spatial coherence in their oscillatory patterns, suggesting a possible connection between the magnetic field topology and oscillatory behavior (Figures 2-4).

The study also examines the Doppler shift in the *IRIS* spectrum, focusing on the propagating periodic oscillation in BPs. The findings indicate that internetwork BPs generally

exhibit lower damping rates and wider velocity ranges compared to network BPs. The investigation also analyzed the damping per period histograms, which showed distinct peaks at specific values for both internetwork and network BPs. Regarding oscillated BPs, network BPs had a narrower damping per period range compared to internetwork BPs. The highest Doppler velocity was observed in network BPs, while oscillated internetwork BPs showed maximum Doppler velocities ranging from 24 to 30 km/s. For non-oscillated BPs, the maximum Doppler velocity was similar between network BPs (20 km/s) and internetwork BPs (35 km/s).

In active region (AR) areas, the study found that internetwork BPs generally exhibit higher damping rates and wider velocity ranges compared to network BPs. The analysis of damping per period histograms identified significant peaks at specific values for both internetwork and network BPs. Regarding oscillated BPs, both network BPs and internetwork BPs had similar damping per period ranges. However, the maximum Doppler velocity range was wider for internetwork BPs compared to network BPs, indicating higher velocity ranges for internetwork BPs. For non-oscillated BPs, the maximum Doppler velocity was similar between network BPs and internetwork BPs. The study focuses on the physical properties and dynamics of network and internetwork BPs in different regions of the Sun. In Quiet Sun areas, network BPs have a damping per period range of 0.3 to 1.5, while internetwork BPs have a range of 0.2 to 1.5. The maximum Doppler velocity range for internetwork BPs is wider, between 10 to 50 km/s, compared to network BPs which have a range of 25 to 40 km/s. The study found dominating peaks at 1.65 ± 0.2 and 0.6 ± 0.2 for internetwork BPs and a dominant peak at 0.4 ± 0.2 for network BPs. The maximum Doppler velocity for oscillated network BPs is 30 km/s, slightly higher than oscillated internetwork BPs which range between 20 to 35 km/s. Non-oscillated network BPs have a maximum Doppler velocity of 20 km/s, similar to non-oscillated internetwork BPs at 40 km/s.

In Coronal Hole areas, internetwork BPs generally have higher damping rates and higher velocity ranges compared to network BPs. The damping per period range for internetwork BPs is 0.1 to 1.6, while for oscillated internetwork BPs, the range is 0.1 to 2.2. The wider velocity range for internetwork BPs suggests that they are subject to more energetic processes or more turbulent flows. The significant peak for internetwork BPs is at 0.6 ± 0.2 , whereas the dominant peak for network BPs is between 0.7 ± 0.2 and 1.1 ± 0.2 . The maximum Doppler velocity for oscillated network BPs is slightly higher than oscillated internetwork BPs at 30 km/s. Non-oscillated network BPs have a higher maximum Doppler velocity at 80 km/s compared to non-oscillated internetwork BPs at 68 km/s.

In Active Regions, internetwork BPs have higher damping rates and higher velocity ranges compared to network BPs. The higher damping rates for internetwork BPs suggest that they are more efficiently damped than network BPs. The wider velocity range for internetwork BPs suggests that they are subject to more energetic processes or more turbulent flows. The study also found that the population of oscillated BPs in AR regions is overall lower than in CH regions.

Overall, the results suggest that there are differences and similarities in the properties of oscillated and non-oscillated BPs in different regions of the Sun. In CH areas, internetwork BPs tend to have lower damping rates and higher maximum Doppler velocities compared to network BPs. In AR areas, internetwork BPs tend to have higher damping rates and wider maximum Doppler velocity ranges than network BPs.

5 Discussion

The study reveals a clear distinction between oscillated and non-oscillated BPs, with oscillated BPs demonstrating significantly higher oscillatory power in the 3-5 minute period range. This is supported by the observation of a higher degree of spatial coherence in their oscillatory patterns, suggesting a potential link between the magnetic field topology and oscillatory behavior. In terms of spectral properties, oscillated BPs were found to exhibit stronger line emission and broader line profiles, indicative of higher temperatures, densities, and velocities. This suggests a correlation between the oscillatory behavior and the heating of BPs, which is a significant finding in understanding the dynamics of these solar phenomena.

Several attempts have been made to demonstrate and directly determine the scaling law of theoretically predicted damping times and compare it with the observed damping times for the MHD oscillation events. However, the small number of detected events does not allow to discriminate between competing damping theories. The spectral observations from the *IRIS* instrument could have significant physical implications, provided that the correct damping mechanism for the Doppler velocity oscillations of BPs is identified.

The damping mechanism of Doppler velocity longitudinal oscillations provides clues to the mechanism of TR and coronal heating. The scaling of the damping time with the parameters of BPs observed in the extreme ultraviolet by the *IRIS* instrument was determined, suggesting a different damping mechanism in the network and internetwork BPs. The analysis of the damping per period and maximum Doppler velocity of BPs in different solar regions (AR and CH) revealed distinct patterns. In AR areas, internetwork BPs showed higher damping rates and wider maximum Doppler velocity ranges compared to network BPs. In CH areas, both types of BPs demonstrated similar damping rates, but internetwork BPs tended to have higher maximum Doppler velocities compared to network BPs.

Understanding the distinctions between NOBPs and OBPs has real uses, as solar BPs can be used to detect magnetic activity on the Sun, which can have a major effect on the Earth's atmosphere and space environment. More research is required to fully comprehend the complex processes at work and investigate the actual applications of these results. The study analyzed the behavior of network and internetwork BPs (BPs) in the solar atmosphere, focusing on their supercritical damping behavior. Supercritical damping occurs when a system loses energy faster than it would without damping, suggesting strong damping processes associated with the interaction of BPs with the surrounding plasma. This is in contrast to findings in active regions and quiet Sun areas, where oscillated network BPs exhibited critical damping behavior and internetwork BPs exhibited supercritical damping behavior, respectively.

The differences in damping behavior between CH, and AR areas suggest that the physical mechanisms responsible for the damping of BPs may depend on local plasma conditions and the magnetic environment. The population of oscillated BPs in AR regions was overall lower than in CH regions, suggesting that the oscillatory behavior of BPs in AR regions may be more influenced by local plasma and magnetic conditions. The lower population of oscillated BPs in AR regions may also be related to the fact that the magnetic fields in these regions are more highly concentrated, which can lead to stronger damping of the oscillations. The study found a significant connection between the oscillatory behavior and the properties of BPs, with oscillations playing a crucial role in the energy transport and heating of these features. Further studies, including numerical simulations and detailed modeling, are needed to understand the underlying physical mechanisms responsible for the observed differences between oscillated and non-oscillated BPs. The classification of BPs into two primary categories, oscillated BPs, and non-oscillated BPs, was investigated. Oscillated

BPs were further classified into network and internetwork subtypes based on their oscillation period times. A machine learning (ML) algorithm, specifically a convolutional neural network (CNN), was utilized to implement the classification of BPs into the aforementioned categories. The training phase involved training the CNN model to identify patterns and features in the images that corresponded to each BP category and subtype, including the oscillation period times falling within the specified ranges. The model was then deployed to classify BPs in new, unseen data, extracting relevant features and predicting the BP type and subtype based on the calculated oscillation period times falling within the respective ranges. In conclusion, the research successfully categorized BPs into oscillated and non-oscillated types, with further classification into network and internetwork subtypes based on oscillation period times.

Authors' Contributions

All authors have the same contribution.

Data Availability

The data that support the findings of this study are available from the corresponding author upon reasonable request.

Conflicts of Interest

The authors declare no potential conflicts of interest.

Ethical Considerations

The authors have diligently addressed ethical concerns, such as informed consent, plagiarism, data fabrication, misconduct, falsification, double publication, redundancy, submission, and other related matters.

Funding

This research did not receive any grant from funding agencies in the public, commercial, or nonprofit sectors.

References

- [1] Nesis, A., Hammer, R., Roth, M., & et al. 2001, *Sol. Phys.*, 200, 11.
- [2] Muller, R., Roudier, T., Vigneau, J., & et al. 1994, *A&A*, 283, 232.
- [3] Falconer, D. A., Moore, R. L., Porter, J. G., & et al. 1998, *ApJ*, 501, 386.
- [4] Berger, T. E., & Title, A. M. 1996, *ApJ*, 463, 365.
- [5] Ugarte-Urra, I., Doyle, J. G., Madjarska, M. S., & et al. 2004, *A&A*, 418, 313.

- [6] Tavabi, E., Ajabshirizadeh, A., Ahangarzadeh Maralani, A. R., & et al. 2015, *A&A*, 36, 307.
- [7] Gao, Y., Tian, H., Van Doorselaere, T., & et al. 2022, *ApJ*, 930, 55.
- [8] Ajabshirizadeh, A., Tavabi, E., & Koutchmy, S. 2009, *Ap&SS*, 319, 31.
- [9] Jess, D. B., Mathioudakis, M., Erdélyi, R., & et al. 2009, *Science*, 323, 1582.
- [10] Tavabi, E., Koutchmy, S., Ajabshirizadeh, A., & et al. 2015, *A&A*, 573, A4.
- [11] Samanta, T., Pant, V., & Banerjee, D. 2015, *ApJ*, 815, L16.
- [12] Sangal, K., Srivastava, A. K., Kayshap, P., & et al. 2022, *MNRAS*, 517, 458.
- [13] Zeighami, S., Tavabi, E., & Amirkhanlou, E. 2020, *A&A*, 41, 18.
- [14] Andic, A., & et al. 2010, *ApJ*, 717, L79.
- [15] Li, T., & Zhang, J. 2016, *A&A*, 589, A114.
- [16] Hou, Z., Huang, Z., Xia, L., & et al. 2016, *Solar Wind* 14, 1720, 020001.
- [17] Tavabi, E. 2018, *MNRAS*, 476, 868.
- [18] De Pontieu, B., Polito, V., Hansteen, V., & et al. 2021, *Sol. Phys.*, 296, 84.
- [19] Kayshap, P., & Dwivedi, B. N. 2017, *Sol. Phys.*, 292, 108.
- [20] Madjarska, M. S. 2019, *Living Reviews in Solar Physics*, 16, 2.
- [21] Sadeghi, R., & Tavabi, E. 2024, *Sol. Phys.*, [[arXiv:2406.05105](https://arxiv.org/abs/2406.05105)].
- [22] Pustovitov, V. D. 2011, *Plasma Physics Reports*, 37, 109.
- [23] Shukla, N., Shukla, P. K., & Stenflo, L. 2009, *Phys. Rev. E*, 80, 027401.
- [24] Vodopyanov, A. V., Mansfeld, D. A., Chekmarev, N. V., & et al. 2020, *Proc. SPIE*, 11582, 115820Z.
- [25] Willett, J. E., & Maraghechi, B. 1977, *Plasma Physics*, 19, 785.
- [26] Zhao, J., Schmieder, B., Li, H., & et al. 2017, *ApJ*, 836, 52.
- [27] Reale, F., Testa, P., Petralia, A., & et al. 2019, *ApJ*, 882, 7.
- [28] Guglielmino, S. L., Zuccarello, F., Young, P. R., & et al. 2018, *ApJ*, 856, 127.
- [29] Sadeghi, R., & Tavabi, E. 2022, *ApJ*, 938, 74.
- [30] Tavabi, E., & Sadeghi, R. 2024, *Advances in Space Research*, 73, 4859.
- [31] Parks, G. K. 2004, *Physics of space plasmas: an introduction*, Westview Press, 2003.
- [32] Tavabi, E., Zeighami, S., & Heydari, M. 2022, *Sol. Phys.*, 297, 76.
- [33] Jansen, F., & Pirjola, R. 2004, *EOS Transactions*, 85, 241.
- [34] Pirjola, R., Kauristie, K., Lappalainen, H., & et al. 2005, *Space Weather*, 3, S02A02.

- [35] Chandrashekhhar, K., Krishna Prasad, S., Banerjee, D., & et al. 2013, *Sol. Phys.*, 286, 125.
- [36] Sadeghi, R., & Tavabi, E. 2022, *MNRAS*, 512, 4164.
- [37] Sadeghi, R., & Tavabi, E. 2023, *Advances in Space Research*, [[arXiv:2406.10720](#)].
- [38] Gao, Y., Tian, H., Van Doorselaere, T., & et al. 2022, *ApJ*, 930, 55.
- [39] Khomenko, E., & Collados, M. 2015, *Living Reviews in Solar Physics*, 12, 6.
- [40] Muller, R., Roudier, T., Vigneau, J., & et al. 1994, *A&A*, 283, 232.
- [41] Sánchez Almeida, J., Márquez, I., Bonet, J. A., & et al. 2004, *ApJ*, 609, L91.
- [42] De Pontieu, B., Title, A. M., Lemen, J. R., & et al. 2014, *Sol. Phys.*, 289, 2733.
- [43] Wülser, J.-P., Title, A. M., Lemen, J. R., & et al. 2012, *Proc. SPIE*, 8443, 844308.
- [44] Kang, K., & Wang, X. 2014, [[arXiv:1411.4464](#)].
- [45] Albawi, S., Mohammed, T. A., & Al-Zawi, S. 2017, *International Conference on Engineering and Technology (ICET)*, 1.
- [46] Chauhan, R., Ghanshala, K. K., & Joshi, R. C. 2018, *First International Conference on Secure Cyber Computing and Communication (ICSCCC)*, 278.

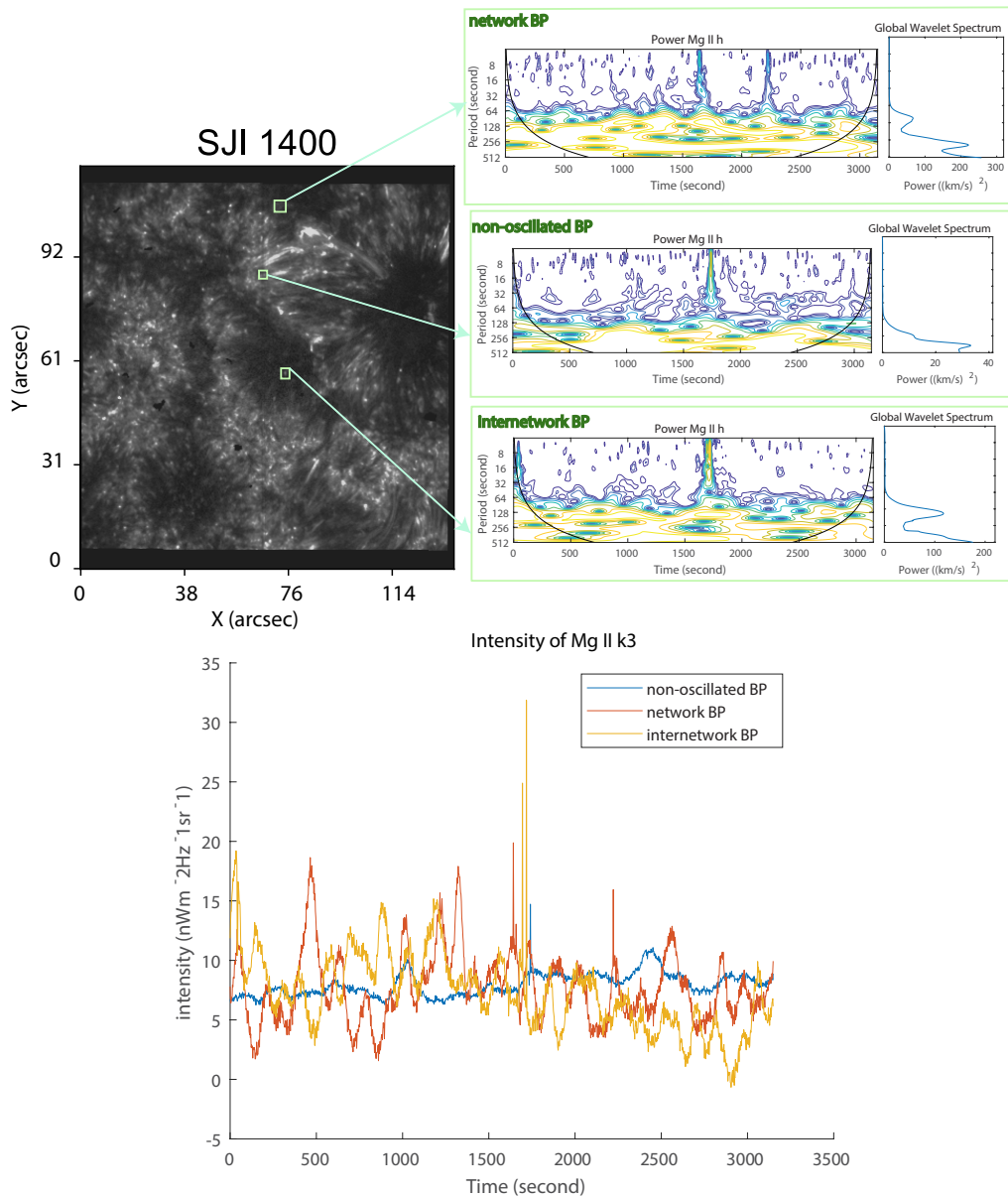


Figure 1: Illustration of three types of BPs on the SJI at 1403 Å wavelength. The BPs consist of a network BP, an internetwork BP, and a non-oscillated BP. The picture also includes a wavelet representing the intensity of Mg II k 3. The graphic depicts the intensity profiles of the network BP, internetwork BP, and non-oscillated BP, offering information about their respective properties and behaviors.

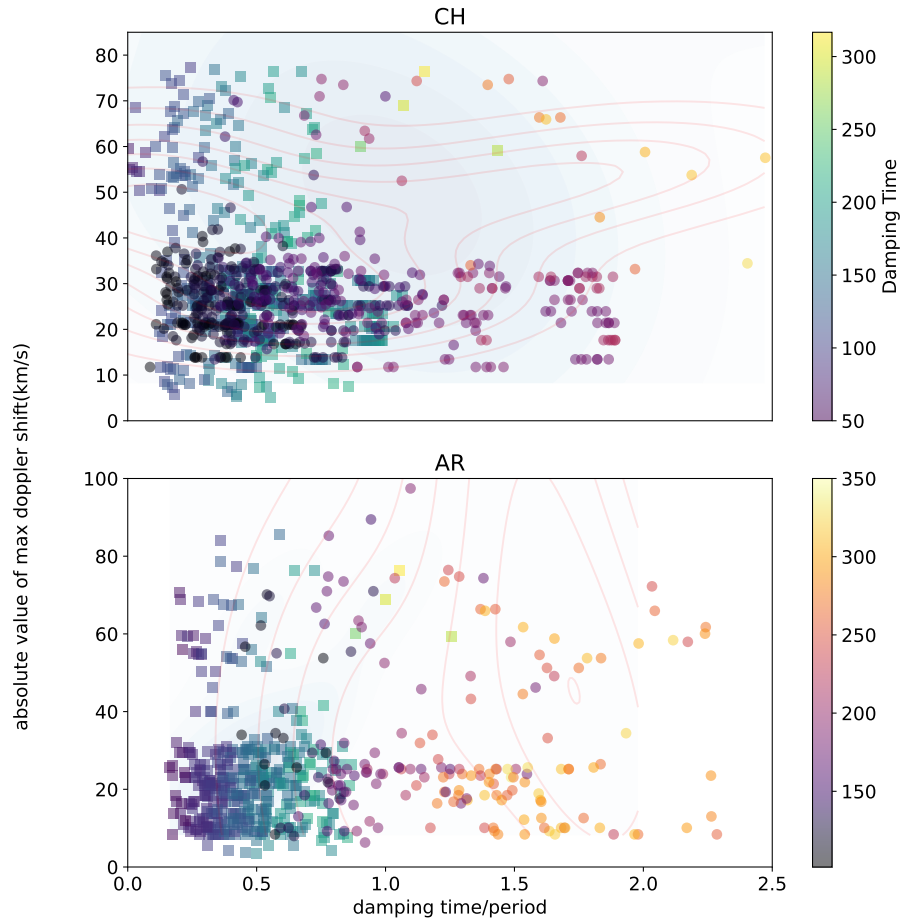


Figure 2: The scatter plot shows the relationship between damping time/period and the number of cases in the network (square markers) and interconnect (circle markers) operating systems. The x-axis represents the damping time normalized by the period, while the y-axis represents the number of cases.

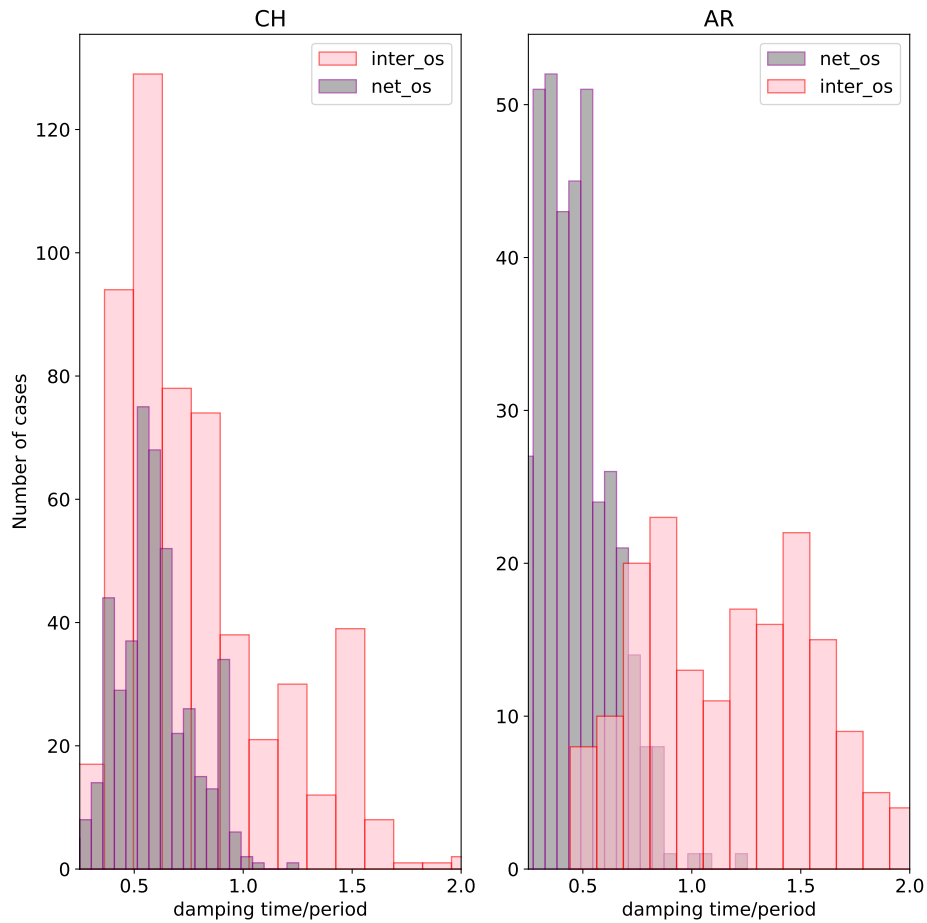


Figure 3: The histogram illustrates the distribution of damping time/period in the network (gray bars) and interconnect (pink bars) operating systems. The x-axis represents the damping time normalized by the period, while the y-axis represents the number of cases. The histogram bars indicate the frequency of occurrence for different damping time/period values.

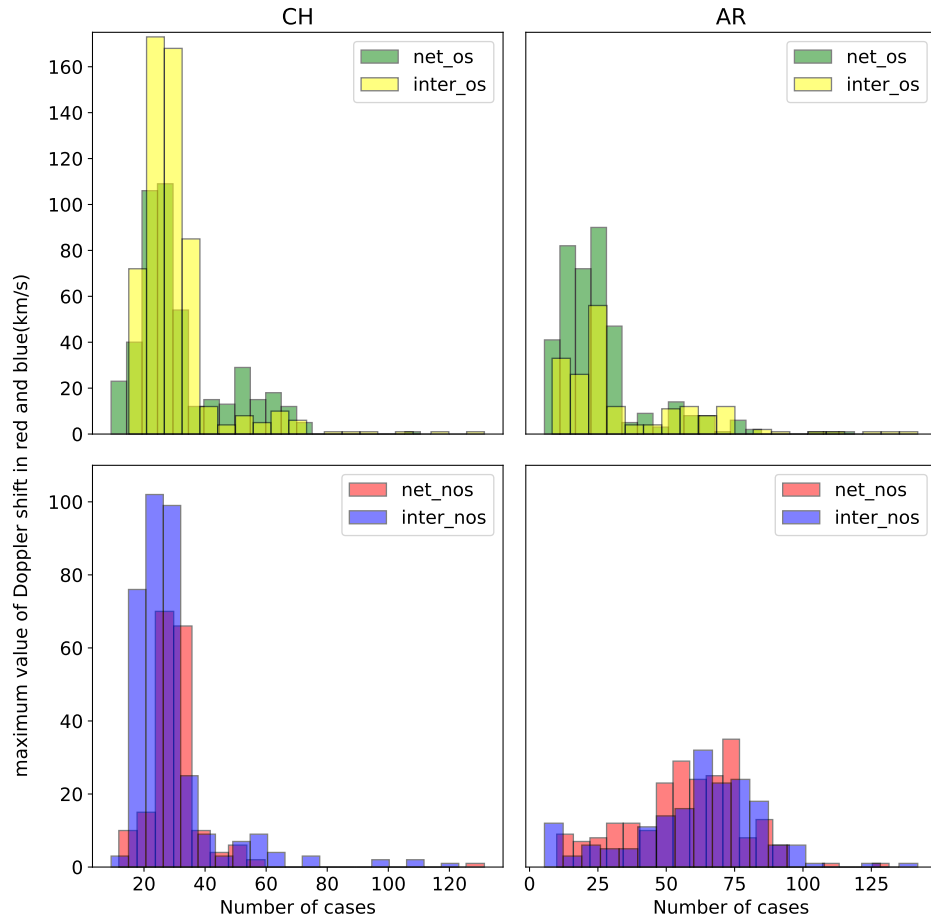


Figure 4: The vertical histograms represent the distribution of the number of cases in different scenarios. The green bars represent the number of cases in the network operating system, the yellow bars represent the number of cases in the interconnect operating system, the red bars represent the number of cases in the network non-operating system, and the blue bars represent the number of cases in the interconnect non-operating system.